Magnetic and transport behavior of electron-doped $La_{1-x}Mg_xMnO_3$ $(0.45 \leqslant x \leqslant 0.6)$

J. H. Zhao, H. P. Kunkel, X. Z. Zhou, and Gwyn Williams
Department of Physics and Astronomy, University of Manitoba, Winnipeg, Canada MB R3T 2N2
(Received 13 March 2002; revised manuscript received 12 August 2002; published 27 November 2002)

Detailed measurements of the linear and nonlinear magnetic responses, the zero-field cooled and field-cooled magnetization, and the resistivity of electron-doped $La_{1-x}Mg_xMnO_3$, $0.45 \leqslant x \leqslant 0.6$, are summarized. For $0.05 \leqslant x \leqslant 0.6$ this system exhibits a single paramagnetic to ferromagnetic phase transition on cooling with no *thermodynamic* reentrant transition to a spin-glass-like phase. Nevertheless, both a detailed analysis of the critical response and the low temperature saturation moment show clear evidence of competing interactions. The latter could arise either as a result of spontaneous electronic phase separation or from conventional noncollinearity (homogeneous, or—due to the random substitution process—inhomogeneous). These results argue against a simple double exchange picture for this system and a uniform ferromagnetic ground state. However, features evident in the zero-field-cooled behavior (and the nonlinear response) at temperatures below T_c originate from technical sources viz. the increase in coercive field, so it is possible that a gradual onset of competing interactions might arise from a related source. The resistivity data confirm that the complete suppression of a metal-insulator transition in these systems with small average *A*-site radius extends into the electron-doped regime ($x \geqslant 0.5$). Thus ferromagnetism dominates but the system remains *insulating*, contrasting with an emerging ferromagnetic *metallic* state for which a spontaneous electronic phase-separation approach has been proposed. Indeed, the transport data conform with model expressions for charge transport by nonadiabatic small polarons in the paramagnetic phase, but they are quantitatively inconsistent with the expression derived recently by Rahkmanov *et al.* [Phys. Rev. B **63**, 174429 (2001)] for the *specific* model of polaronic hopping in a nonmetallic, phase separated picture.

DOI: 10.1103/PhysRevB.66.184428 PACS number(s): 75.40.Cx, 75.30.Kz, 75.30.Vn, 72.80.Ga

I. INTRODUCTION

A recent paper[1] presented a summary of detailed magnetic and transport measurements on hole-doped $La_{1-x}Mg_xMnO_3(0.05 \leqslant x \leqslant 0.4)$, based on which a tentative phase diagram was proposed. In those and the present specimens the average *A*-site radius $\langle r_A \rangle$ is low enough to completely suppress the appearance of a metal-insulator transition over the entire doping range studied, a result that presumably reflects an associated reduction in the Mn $e_g - O(2p_\sigma)$ bandwidth, which persists despite the continued presence of magnetic ordering at low temperature. Furthermore, while the declining saturation moment fits qualitatively into the recently advocated electronic phase separated model for magnetoresistive manganites, in which colossal magnetoresistance arises through a field dependent percolative linkage of a ferromagnetic metallic backbone embedded in an antiferromagnetic insulating matrix,[2] the result that ferromagnetism dominates but the system remains insulating contrasts with the situation to which this model has been widely applied. In particular, the resistivity data are quantitatively inconsistent with predictions made recently by Rakhmanov *et al.*[3] for the specific case of conduction based on magnetic small polarons existing in a nonmetallic phase-separated environment.

The detailed magnetic measurements also revealed complications, yielding asymptotic critical exponent values consistent with those predicted by the isotropic, near-neighbor Heisenberg model[4] ($\gamma = 1.386$, $\beta = 0.365$, and $\delta = 4.80$) at low doping levels ($x \leqslant 0.33$). However, the presence of site disorder, linked with the process of cation substitution, and presumably resulting in a distribution of exchange coupling parameters $P(J)$ between interacting Mn spins, modified *effective* exponent values away from the critical point[5] ($H \rightarrow 0, T \rightarrow T_c$). It was suggested that this would result if the ratio $\eta = J_0/J$ of the first (J_0) to second (J) moment of the (assumed) Gaussian distribution $P(J)$ declined rapidly towards unity as $x \rightarrow 0.4$. The effects of the latter are well known to reduce the region of validity of true (asymptotic) critical behavior in the (H-T) plane[6].

Below we summarize the results of both magnetic and transport measurements, complemented by an investigation of the nonlinear magnetic response, on the electron-doped region of this system, specifically $0.45 \leqslant x \leqslant 0.6$. These reveal some similarities, but some striking differences from those reported for the hole-doped regime.

II. EXPERIMENTAL DETAILS

Three samples, with nominal compositions of $x = 0.45$, 0.5, and 0.6, were prepared in the same manner as those for lower x.[1,7] Room temperature x-ray diffraction data, acquired using Cu $K\alpha$ radiation in equipment previously described,[7] revealed a single-phased orthorhombic structure ($Pbnm$) with $c/\sqrt{2} < a < b$, as expected, comparable to those reported previously for $x = 0.4$. Additionally the full width at half maximum of the (020) reflection near $\theta = 32.9°$ was found to lie in the range 0.15–0.20° for all samples investigated ($0.05 \leqslant x \leqslant 0.6$), comparable to that reported earlier[8] for the similarly prepared polycrystalline ceramic $La_{0.67}Ca_{0.33}MnO_3$. Furthermore, no evidence for the presence of the oxides of manganese, specifically Mn_3O_4, and MgO, were detected above the background (which places an upper limit of around 1 wt % on them[9]). Such oxides would

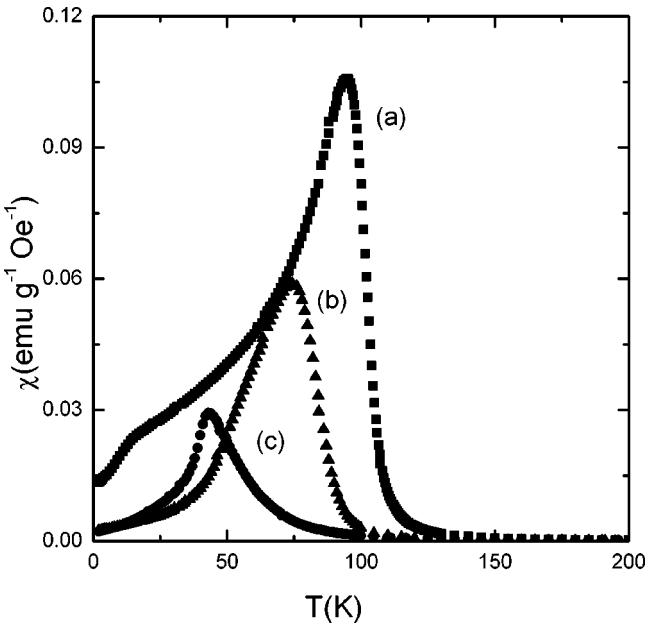

FIG. 1. The zero-field ac susceptibility χ $(0,T)$, corrected for background and demagnetizing effects, plotted against temperature T (K), for (a) $x=0.45$, (b) $x=0.5$, and (c) $x=0.6$.

necessarily form as impurity phases if Mg failed to replace La at the *A* site in this system. A more stringent limit on the extent of such phases is provided by the magnetic data (specifically Figs. 1–4, 9, 10, and 12); Mn_3O_4 orders[10] near 40 K producing a strong characteristic signature in the ac susceptibility.[11] Similar features are expected from the mixed

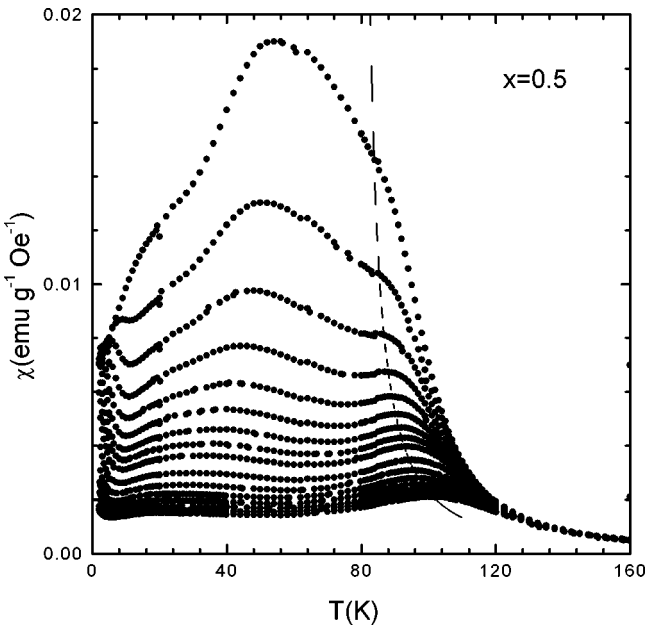

FIG. 2. The ac susceptibility χ (H,T), of the $x=0.5$ sample, measured in superimposed static biasing fields (increasing from top to bottom) of 300–1000 Oe (in 100-Oe steps) and 1200–2600 Oe (in 200-Oe steps) plotted against temperature. The dashed line—the locus of the critical maxima— delineates the crossover line in the (H - T) plane.

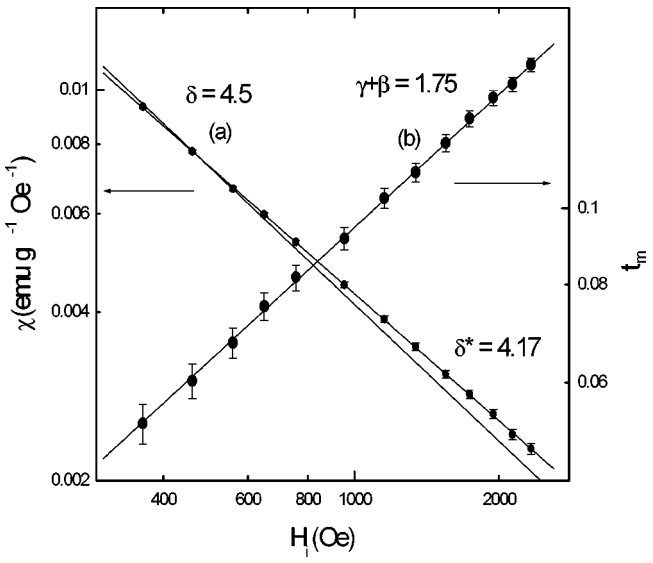

FIG. 3. (a) The critical peak amplitude, taken directly from data similar to Fig. 2 for the $x=0.45$ specimen, plotted against the internal field H_i on a double logarithmic scale. The solid line—a fit to the first three points—yields $\delta=4.5$, while the dashed line—a fit to all points—yields $\delta^*=4.17$ (see the text for a discussion). (b) A double-logarithmic plot of the (reduced) critical peak temperature t_m, taken from data similar to that in Fig. 2, against the internal field H_i (in Oe). The solid line drawn confirms the power-law prediction of Eq. (2), and its slope yield $(\gamma+\beta)=1.75$.

oxide $MgMnO_3$ which orders at lower temperature[12] and from self-doped $La_{1-x}MnO_3$ which becomes ferromagnetic[11,13] below about 180 K. No such features were observed, limiting the presence of such impurity phases in the

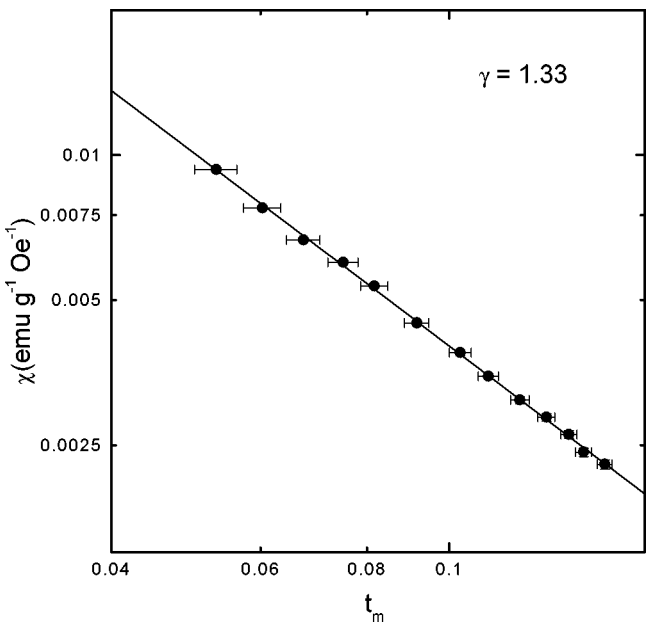

FIG. 4. The critical peak amplitude from data similar to Fig. 2 for the $x=0.45$ specimen plotted against reduced temperature t_m on a double-logarithmic scale. The line drawn confirms the power law prediction of Eq. (3) and its slope yields $\gamma=1.33$.

TABLE I. Ferromagnetic ordering (T_c) and paramagnetic Curie (θ) temperature, Hopkinson maximum susceptibilities [$\chi(0,T_H)$], effective moments (P_{eff}), and exponent estimates.

x	0.45	0.5	0.6
T_c (K)	98.5±0.5	79±0.5	46±1
$\gamma+\beta$	1.75±0.09	1.78±0.13	1.73±0.09
	($400 \leqslant H_i \leqslant 2.2$ kOe)	($400 \leqslant H_i \leqslant 2.4$ kOe)	($600 \leqslant H_i \leqslant 3$ kOe)
γ	1.33±0.06	1.28±0.07	1.25±0.08
	($t_m \geqslant 0.05$)	($t_m \geqslant 0.1$)	($t_m \geqslant 0.3$)
δ	4.5±0.4	4.2±0.6	4.15±0.7
	($400 \leqslant H_i \leqslant 700$ Oe)	($400 \leqslant H_i \leqslant 700$ Oe)	$600 \leqslant H_i \leqslant 900$ Oe)
δ^*	4.17±0.2	3.65±0.17	3.65±0.3
	($400 \leqslant H_i \leqslant 2.2$ kOe)	($400 \leqslant H_i \leqslant 2.4$ kOe)	($600 \leqslant H_i \leqslant 3$ kOe)
θ (K)	149	162	126
$\chi(0, T_H)$(emu g^{-1} Oe^{-1})	0.11	0.06	0.03
$P_{eff}(\mu_B)$	4.5(7)	4.5(0)	4.3(2)

present samples to a factor of 2–3 lower than the upper limit set by the x-ray data. Indeed, the deliberate replacement of Mn by Mg in this system leads to an increase[14] in the ferromagnetic ordering temperature T_c, the opposite to the trend reported below; the present results agree with a reported reduction in T_c as the average A-site radius $\langle r_A \rangle$ decreases.[15,16] The present polycrystalline ceramic specimens displayed average grain sizes of typically 2–4 μm, estimated as detailed previously.[8] No other means of structurally characterising these samples is available to us currently.

Samples of comparable dimensions—approximately $1 \times 1 \times 7$ mm^3—were utilized in all the magnetic and transport measurements. The former were acquired in a Quantum Design PPMS model 6000 system, and the latter using a conventional four-probe technique.

III. RESULTS AND DISCUSSION

A. Linear magnetic response

The zero-field ac susceptibility (measured on warming, following zero-field cooling, at 2.4 kHz with a driving field amplitude of 0.03 Oe applied along the largest sample dimension) increases rapidly with decreasing temperature, as shown in Fig. 1 (no thermal hysteresis was detected). $\chi(0,T)$ then peaks below the ferromagnetic ordering temperature (T_c) (as subsequent discussion confirms) at the principal (Hopkinson) maximum[17] (at temperature T_H). Below T_H, $\chi(0,T)$ falls essentially monotonically as the temperature is further reduced. Two important features are revealed by the data in this figure: (i) The peak susceptibility $\chi(0,T_H)$ falls rapidly with increases in the Mg composition x in this range (Table I summarizes these susceptibilities). Such behavior is reminiscent of the effects of increasing exchange bond disorder leading to the suppression of ferromagnetism and its replacement by a spin-glass-like phase.[18] (ii) when viewed on an expanded scale, no signal arising from any of the impurity phases mentioned above could be detected.

B. Field-dependent ac susceptibility

Figure 2 reproduces the field- and temperature-dependent ac susceptibility of the $x=0.5$ specimen in applied fields (H_a) up to 2–3 kOe (these static biasing fields were applied parallel to the ac driving field). This figure is in marked contrast to those reported at lower x, it displays far more structure, with characteristic features at both high and low temperatures.

1. Ferromagnetic transition

Certain high temperature features, evident in this figure, are common to all three samples—a series of peaks that move upward in temperature but decrease in amplitude with increases in H_a once the latter has increased sufficiently to suppress the Hopkinson maximum in amplitude and (downward in) temperature (i.e., $H_a \geqslant 400$ Oe). Such peaks, the locus of which is delineated by the dashed line, signal a (continuous) transition to a ferromagnetic state. This conclusion follows from an analysis of the corresponding peak structure based on the static scaling law[19,20] and Monte Carlo simulations of the three-dimensional Heisenberg model,[21] implemented below, enabling estimates of the usual critical exponents γ, β, and δ to be determined from the peak behavior, as discussed in detail previously for metallic, amorphous, and semiconducting systems;[22] thus the main conclusions alone are presented below:

(a) Figure 3(a) shows the critical peak amplitude $\chi(H_i,T_M)$ taken directly from data similar to that shown in Fig. 2 (corrected for demagnetizing and background effects) plotted against the internal field H_i ($=H_a-NM$ in the usual notation, with N estimated from the shearing curve) on a double logarithmic scale for $x=0.45$ sample. The scaling law approach predicts a power-law relationship between these quantities, viz.

$$\chi(H_i,T_M) \propto H_i^{1/\delta-1}, \tag{1}$$

which allows a value for δ to be found, *independent of any knowledge or a choice for* T_c. A close examination of this figure reveals some curvature, attributed to exchange bond disorder (discussed in more detail below). A least squares fit to the first three points (the *low* field region) yields

$$\delta = 4.5 \pm 0.4 \quad (400 \leqslant H_i \leqslant 700),$$

consistent—within the listed uncertainty—with Heisenberg model values. Fitting the entire data set in this figure yields a lower effective/average value of

$$\delta^* = 4.2 \pm 0.2 \quad (400 \leqslant H_i \leqslant 2.2 \text{ kOe}).$$

(b) Figure 3(b) reproduces a double logarithmic plot of the reduced critical peak temperature t_m (also taken from similar data to Fig. 2) against the internal field H_i; the scaling approach predicts

$$\frac{T_M - T_c}{T_c} = t_m \propto H_i^{(\gamma+\beta)^{-1}}. \tag{2}$$

The line drawn—a least squares fit—confirms the power-law prediction of Eq. (2) and yields

$$\gamma + \beta = 1.75 \pm 0.09 \quad (400 \leqslant H_i \leqslant 2.2 \text{ kOe}).$$

(c) Finally the predicted power-law relationship between the critical peak amplitude $\chi(H_i, T_M)$ (directly from data similar to Fig. 2) and the (reduced) peak temperature t_m (also found from the same figure),

$$\chi(H_i, T_M) \propto t_m^{-\gamma}, \tag{3}$$

is appraised in Fig. 4. This power law is also confirmed and a least-squares fit of the slope gives

$$\gamma = 1.33 \pm 0.06 \quad (t_m \geqslant 5 \times 10^{-2}).$$

Both these latter relationships rely on a choice for T_c which is found by extrapolating the peak temperatures T_M taken from Fig. 2 to $H_i = 0$. Small adjustments ΔT_c in T_c [$\Delta T_c / T_c \sim (2-4) \times 10^{-3}$] are utilized until consistency is achieved between plots similar to Figs. 3(b) and 4, as discussed previously.[1,5,7] Both of these figures use $T_c = 98.5$ K (with an uncertainty in T_c of ± 0.5 K). These estimates for γ, β, and δ agree—within experimental uncertainty—with $3d$ Heisenberg model values, and hence satisfy the Widom relation $\gamma = \beta(\delta - 1)$, provided, of course, that use is made of the low field estimate for δ (as indeed would be appropriate since critical exponent values characterize the asymptotic behavior). The results obtained from a similar analysis of the data for $x = 0.5$ and 0.6 are summarized in Table I. Effective δ values which decrease in the manner shown in this table are frequently linked to increasing exchange bond "disorder,"[5,20,22] specifically a change in the variance/second moment J in the (assumed) Gaussian distribution of exchange interactions $P(J)$ describing the coupling between Mn spins as the composition x is varied. There are a number of potential causes for such an effect; spontaneous electronic phase separation[2] into ferromagnetic/metallic and antiferromagnetic/insulating regions could underlie such a change, as might the inherently mixed valent nature of these systems through changes in the corresponding Mn^{3+}/Mn^{4+} fraction and their associated interactions—double exchange, superexchange etc.—or conventional noncollinearity associated with the random substitution process. The above data trends do not distinguish between these various possibilities. While the effects of such "disorder" do not change the true *asymptotic* critical behavior ($h \to 0, t \to 0$)—in agreement with the Harris criterion.[23]—it is known to reduce *effective* exponent values *away* from the critical point ($h > 0, t > 0$) in a manner consistent with that reported above and in other systems.[5,20,22]

The suggestion that the ratio η is close to unity in the composition range studied here is supported—at least superficially—by the low temperature structure evident in Fig. 2 and comparable data for $x = 0.45$ and 0.6. This behavior is examined in more detail below.

2. Potential transitions at low temperature

In mean-field models,[24,25] the decline in the ratio η below a value of 5/4 produces subsequent, lower temperature transitions, referred to as reentrant behavior. Below a paramagnetic to ferromagnetic transition of a conventional nature (apart from the modifications to the effective exponents by the presence of exchange bond disorder as described above), vector mean-field models predict the appearance of a "reentrant" phase in which longitudinal ferromagnetic order coexists with transverse spin-glass (random) freezing of spin components (indeed, spin glass behavior has been reported, for example,[26] in both $YCaMnO_3$- and Cr-doped $LaSrMnO_3$). Random transverse spin freezing, linked with the Gabay-Toulouse (GT) line.[27] in the (HT) plane which reflects replica symmetry breaking and weak irreversibility, has a phase boundary described by[28]

$$T_{GT}(0) - T_{GT}(H) = AH^n, \tag{4}$$

with $n = 1$. At still lower temperatures a crossover from weak to strong irreversibility is predicted by these same models on crossing the de Alemeida-Thouless (AT) line in the (HT) plane, defined by a similar equation[29] with $0 < n < 1$.

All of the possible features evident at low temperatures in Fig. 2 and related data for $x = 0.45$ and 0.6 have been examined as possible candidates to associate with these boundaries. As an example the peak structures originating near 60 and 40 K for $x = 0.5$ and 0.6, respectively have been compared with the predicted dependence(s) in Eq. (4). Figure 5 reproduces the variation of this peak temperature, T_p, with field, for the $x = 0.5$ specimen, showing that these data fall into two distinct groups for applied fields above and below about 1 kOe. While either segment of this figure is in general agreement with the linear field dependence of Eq. (4) with $n = 1$ (the GT line), these data, overall, clearly are not. Furthermore the parameters found from such fits:

$$T_{GT}(0) = 58 \pm 1 \text{ K}, \quad A/k_B \sim -3 \times 10^{-2} \text{ K/Oe} \quad (H_a < 1 \text{ kOe}),$$

$$T_{GT}(0) = 37 \pm 1 \text{ K}, \quad A/k_B \sim -7 \times 10^{-3} \text{ K/Oe} \quad (H_a > 1 \text{ kOe}),$$

yield the coefficient(s) A ($= g\mu_B \sqrt{2}[(m^2 + 4m + 2)/4(m + 2)^2]$, where m is the spin dimensionality), in marked dis-

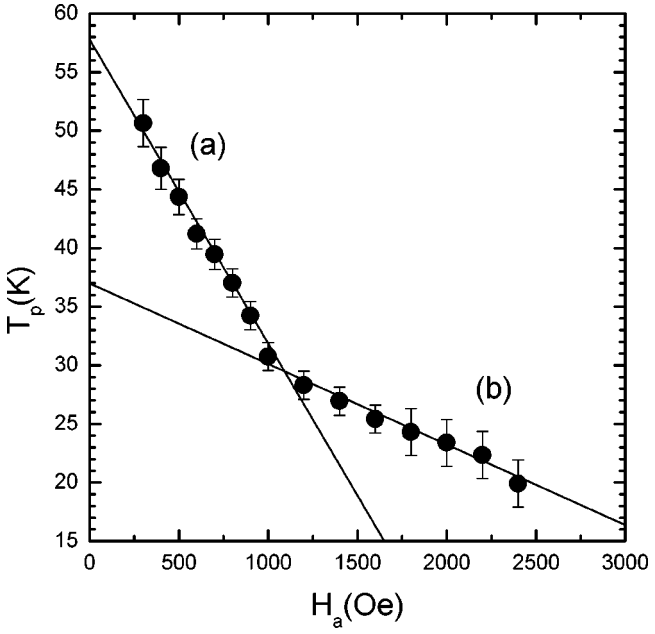

FIG. 5. A plot of the low temperature peak position T_p (in K), against field H_a (in Oe) for the $x=0.5$ sample (Fig. 2). The intercepts and slopes of the two straight lines drawn (a) and (b) are discussed in the text.

agreement with a model value of about -4×10^{-5} K/Oe. A similar behavior, with comparable discrepancies, exists at $x=0.6$.

Both the $x=0.5$ and 0.6 samples also exhibit a trough-like feature at still lower temperature (T_T), but no additional peak structure above 1.8 K. For both $x=0.5$ and 0.6, T_T vs H_a, plots show the concave behavior consistent with the functional form of Eq. (4) with $0\leqslant n\leqslant 1$. The corresponding double logarithmic fits, presented in summary form only, yield, for $x=0.5$,

$$T_{AT}(0)=15.9(5)\ \text{K},\quad B\ [=T_{\text{AT}}(0)A]=1.4\times10^{-2},\quad n=0.5$$

and, for $x=0.6$,

$$T_{AT}(0)=9.5\ \text{K},\quad B=10^{-3},\quad n=0.78.$$

While both appear to reasonably reproduce these data, the fitting parameters are at variance with model predictions. A mean-field approach[27] yields $n=2/3$, while Monte Carlo simulations[30] suggest $n=0.55$–0.7. Both fits yield estimates for n quite different from the mean-field result, with that obtained for $x=0.5$ also lying *below*, but that at $x=0.6$ *above*, the Monte Carlo range. In addition the parameter B exceeds model values by almost an order of magnitude for both systems.

The above analysis and discussion thus indicates that neither of the low temperature features investigated conform in detail to vector model predictions for either the GT or AT phase boundary. Indeed these features likely originate from magnetic technical sources (domain wall motion, coherent domain rotation, etc.), rather than critical effects. This is particularly so for the feature shown in Fig. 5 which originates near the Hopkinson peak. This point is discussed further in relation to the temperature dependence of the magnetization.

3. Nonlinear response

The magnetic response of these samples was also probed by examining the nonlinear magnetic behavior using an ac exiting field $H=H_0\sin\omega t$. The magnetization M produced by this field, being odd in the latter, can be expressed as a corresponding power series[31]

$$M=\chi_0 H+\chi_2 H^3+\chi_4 H^5+\cdots, \tag{5}$$

in which the "susceptibilities" χ_0, χ_2, χ_4, etc., alternate in sign, as they do, for example, in the Brillouin function. The fundamental (M_1), the third harmonic (M_3), etc., are related to these susceptibilities as discussed in Ref. 31: Figure 6 reproduces the measured M_3 for both hole- and electron-doped samples, viz. $0.33\leqslant x\leqslant 0.6$. For signal-to-noise considerations, $H_0$was 10 Oe (with $\omega=300$ Hz); the effects of requiring a relatively large H_0 are discussed better. From this figure it can be seen that this nonlinear response exhibits essentially a two-peaked structure for $0.33\leqslant x\leqslant 0.45$ (with a similar behavior at lower x), a very small second peak at $x=0.5$ and a single peak at $x=0.6$. Standard scaling theory applied to a conventional paramagnetic to ferromagnetic transition relates the (reduced) magnetization m to the usual linear scaling fields $h\propto H_i/T_c$ and $t=|T-T_c|/T_c$ via

$$m=t^{\beta}F\left(\frac{h}{t^{\gamma+\beta}}\right)=t^{\beta}\left(\frac{h}{t^{\gamma+\beta}}-\frac{h^3}{t^{3\gamma+2\beta}}+\cdots\right). \tag{6}$$

Equation (6) indicates that while $\chi_0=m/h$ $(h\to0)$ diverges as $t^{-\gamma}$, a well known and often utilized result χ_2—hence M_3—diverges as $t^{-3\gamma-2\beta}$ as $T\to T_c$. The latter has been verified previously.[32] The higher temperature peaks evident in Fig. 6 reflect this divergence as they occur close to the T_c values estimated for each of these samples using the more conventional methods of Sec. III A 1. Figure 7 illustrates this effect in more detail for $x=0.33$; this figure reproduces a plot of M_3 vs t (using the previously[1] determined value of T_c of 118 K) on a double logarithmic scale. The line drawn corresponds to $t^{-3\gamma-2\beta}$ using Heisenberg model exponents $(3\gamma+2\beta=4.89)$, which fits these data quite well. Expected deviations are observed above $t\sim10^{-1}$ as one passes out of the critical region, while those occurring below $t\sim10^{-2}$ reflect the use of a large exciting field which "mixes" terms in χ_4 into M_3 (Ref. 31), which, being of opposite sign, cause these data to fall below predicted values;[30,32] this effect becomes more pronounced as $T\to T_c$. Other samples studied show this effect to a greater degree than the $x=0.33$ specimen. Of more interest here, however, is the second peak at lower temperature. Several systems that are regarded as potentially reentrant exhibit such a double-peak structure,[5,33] with the lower peak signaling a possible transition into the reentrant phase described above. This view persists, despite the fact that a double-peaked structure in χ_2 (or M_3) is *not* a prediction of broken-symmetry models.[24] Such a behavior is,

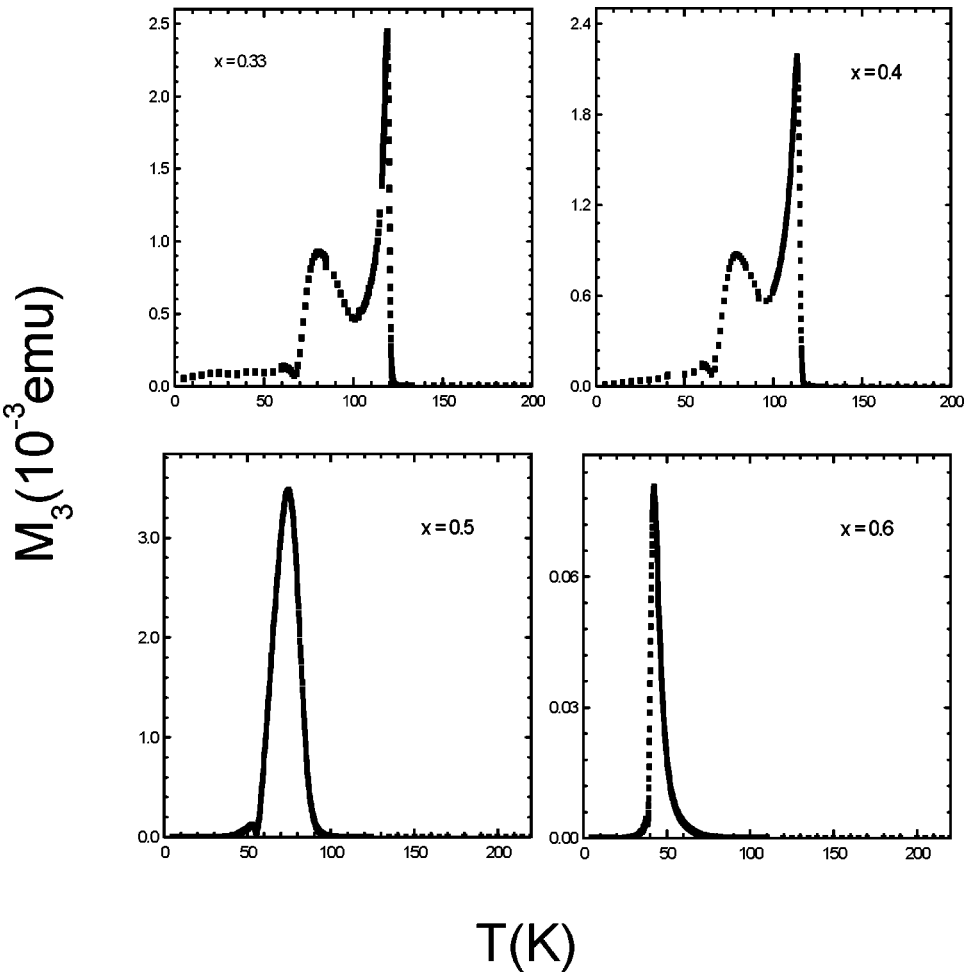

FIG. 6. The third harmonic M_3 (in emu), in the magnetization, plotted against temperature T (K), for specimens with x between 0.33 and 0.6.

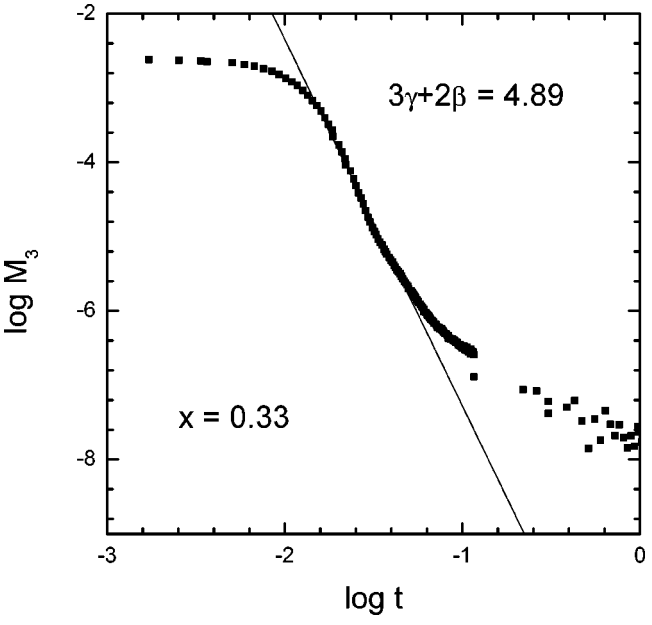

FIG. 7. A double-logarithmic plot of the third harmonic M_3 (in emu), in the magnetization against reduced temperature t for the $x=0.33$ sample. The solid line corresponds to Heisenberg model exponent values $(3\gamma+2\beta)=4.89$.

however, present in mean-field Ising models.[34] Specifically, the lower peak in χ_2 (or M_3) is frequently taken as indicating the temperature at which the system enters the reentrant phase. Such (second) peaks might therefore be used to map this lower phase boundary as a function of composition; detailed comparisons between (Ising) model predictions and experiments again reveal problems. First, the strength of the divergence/anomaly at the lower temperature (reentrant) boundary in model generated data is stronger than that at the upper (paramagnetic to ferromagnetic) one; Fig. 6 shows this not to be the case here. Second, the temperature of the lower peak in M_3—expected to occur on crossing the GT (or possibly the AT) line, should therefore correspond with other estimates for $T_{GT}(0)$ [or $T_{AT}(0)$], a comparison indicates no such correspondence. Thirdly, in potentially reentrant systems previously studied, the (lower) anomaly in M_3 is frequently linked with a characteristic feature in $\chi(0,T)$—often a rapid decrease in the latter;[5,18,33] this does not occur here.

In summary, therefore, M_3 displays features which are superficially consistent with sequential phase transitions. Detailed comparisons show this not to be the case. We contend that the behavior reported above is technical, not critical, in origin (i.e., from domain wall motion or coherent domain rotation, etc. as has been suggested in other cases[33]). This conclusion is consistent with magnetic phase diagrams constructed on the basis of size mismatch at A sites, specifically

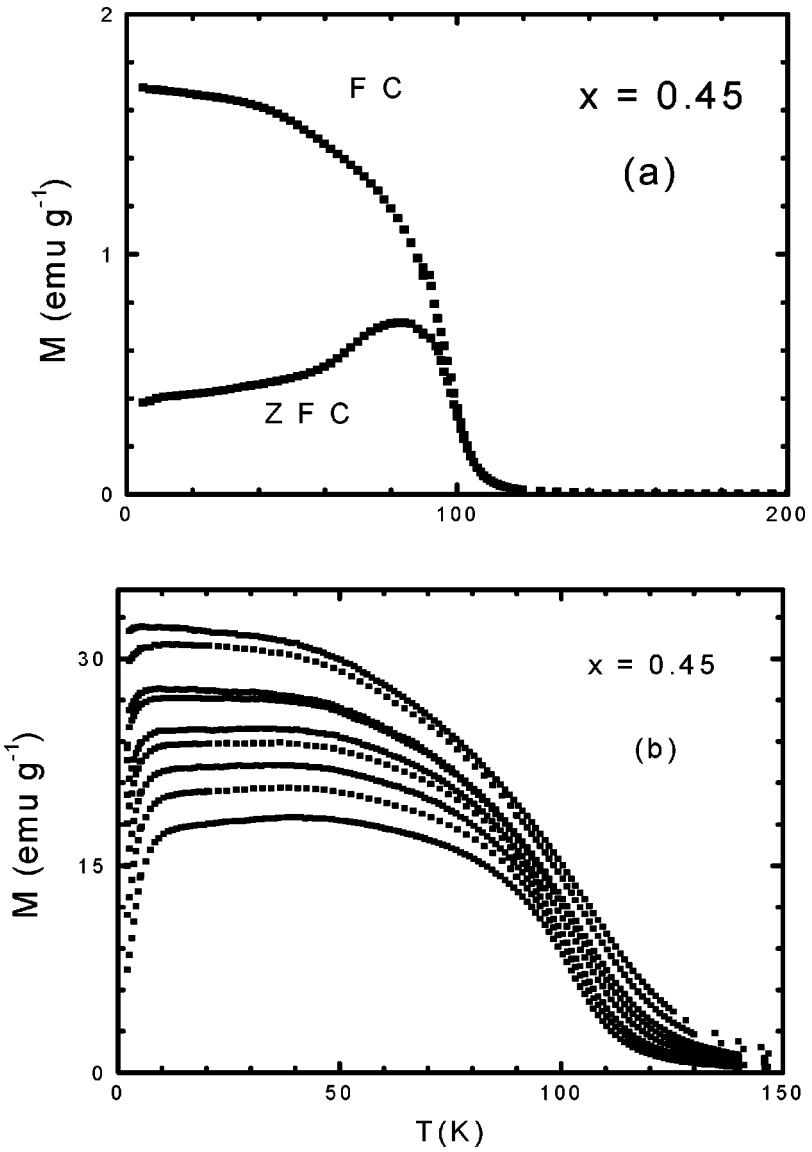

FIG. 8. (a) The zero-field-cooled (ZFC) and field-cooled (FC) magnetizations M (in emu g^{-1}), measured in an applied field of 10 Oe, and (b) the zero-field-cooled magnetizations M (in emu g^{-1}), measured in applied field increasing from 400 Oe (bottom) to 3 kOe (top), both plotted against temperature, T (in K) for the $x=0.45$ sample.

the variance σ^2, in the latter.[35] Here $\sigma^2=1.9\times10^{-4}$ nm^2 at $x=0.5$ (assuming a ninefold coordination for the Mg^{2+} ion; σ^2 decreases for a twelvefold coordination), a value too *small* to produce a spin-glass insulating ground state. The latter reemphasizes the ferromagnetic insulating character of the low temperature state of the present system. This contention is supported by an examination of the following section.

4. Low-field magnetization

Figure 8(a) shows the zero-field cooled (ZFC) and field-cooled (FC) magnetizations for $x=0.45$ sample as a function of temperature in an applied field of 10 Oe (similar data have been collected at $x=0.5$ and 0.6). An examination of these data—and indeed similar ZFC and FC curves[1] for $0.05\leqslant x\leqslant0.4$—indicates that the lower peak in M_3 corresponds to the temperature at which the onset of the rapid decline in the ZFC branch of these curves occurs. The latter was used to delineate a *possible* lower phase boundary on a tentative phase diagram proposed for this system, and the location of this boundary (Fig. 12 of Ref. 1) is in excellent agreement not only with data for $0.05\leqslant x\leqslant0.4$, but also those contained in Figs. 6 and 8. In particular, the estimated T_c of 46 K in the $x=0.6$ sample is in close proximity to the very rapid decline in the corresponding ZFC branch; hence the observation of a single peak in M_3 at this composition. This rapid decline in the ZFC branch has been shown previously to correlate with an attendant increase in the coercive field $H_c(T)$—a magnetic technical effect[7,36]—hence the contention that the lower peaks in $M_3$are of technical—not critical—origin. The bifurcation of the ZFC and FC branches of the magnetization curves necessarily leads to a time dependence in the magnetic response below the bifurcation temperature; however such a time dependence is *not* a characteristic signature solely of a spin-glass state. As demonstrated recently,[36] it is a more general feature associated with a corrugated free energy landscape that can occur not only in *any* magnetically ordered state but also in superparamagnetic systems.

Support—albeit of a qualitative nature—for this association is provided by the ZFC magnetization in fields between 400 and 3 kOe shown in Fig. 8(b) and the temperature varia-

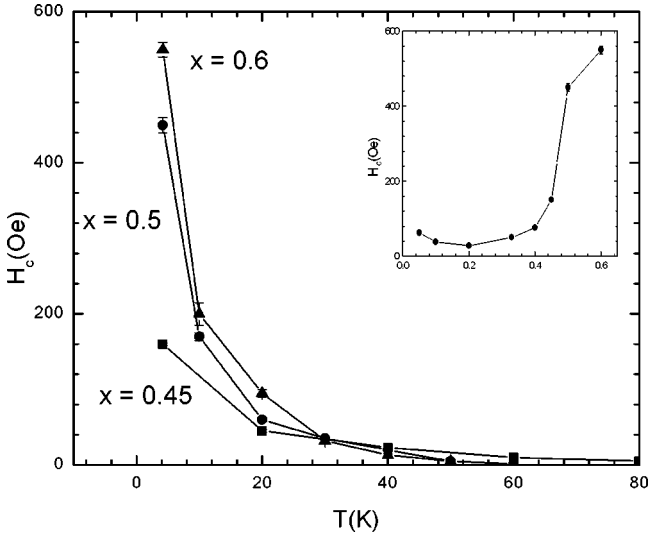

FIG. 9. The temperature dependence of the coercive field H_c (in Oe), for $x=0.45$, 0.5, and 0.6. The inset shows the variation of the coercive field H_c (in Oe), at 4.2 K with composition x for $0.05 \leqslant x \leqslant 0.6$.

tion of $H_c(T)$ (deduced from hysteresis loops) shown in Fig. 9 for the three samples with $x=0.45$, 0.5, and 0.6. In general, the decrease in these magnetization curves with decreasing temperature well below T_c reflects the increasing coercive field shown in Fig. 9. An attempt has been made therefore to correlate features in the magnetization data with model predictions discussed in Secs. III B 2 III B 3. Close examination of Fig. 8(b), however, shows that the temperature at which various features emerge—the fall in the magnetization at lower temperatures, for example—cannot be quantified with nearly the precision that analogous features in $\chi(H,T)$ utilized in Sec. III B 2 could be defined.

The inset in Fig. 9 presents a summary of $H_c(T)$ at 4.2 K as a function of composition x, where the rapid increase in this parameter at $x=0.5$ and beyond leads to the behavior summarized in Fig. 10, the modified phase diagram. In the latter the upper boundary—marked with a solid line—designates a true *thermodynamic* transition (one of a second order/continuous nature) between a paramagnetic insulating phase and a ferromagnetic insulating, low temperature regime. The lower ''boundary''—shown by the dashed line—does not represent such a thermodynamic transition; it simply marks the onset of a marked *technical* magnetic hardness. The coalescence of the two ''boundaries'' at $x=0.5$ simply reflects the marked increase in H_c with x shown in Fig. 9.

This modified phase diagram is considerably simpler than that constructed for other systems, particularly[37] $La_{1-x}Ca_xMnO_3$. Part of this simplification results from the small average A-site radius $\langle r_A \rangle$, accompanying Mg substitution. This completely suppresses the metal-insulator transition at *all* compositions studied, as discussed below. Figure 11 displays the saturation moment deduced from magnetization curves taken at 4.2 K (these moments were estimated by extrapolating M vs H^{-1} plots to the origin of the latter, $H=\infty$); this moment per unit mass *declines* with increasing x,

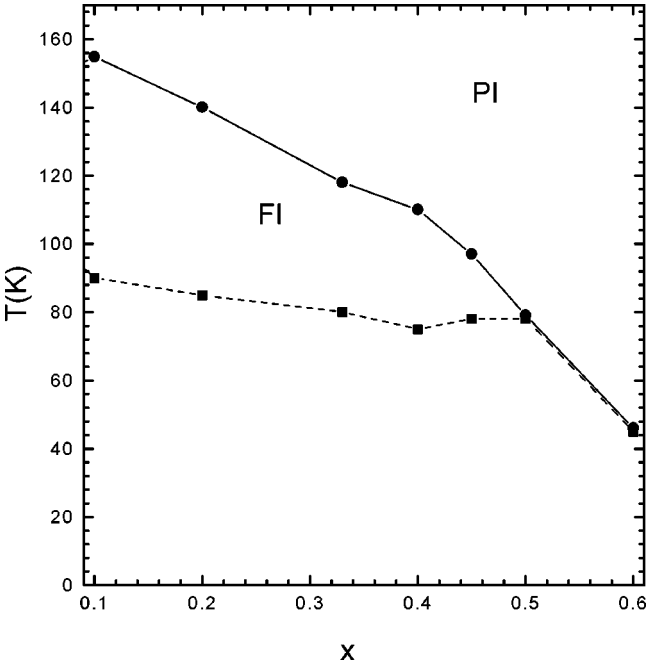

FIG. 10. A modified phase diagram for the $La_{1-x}Mg_xMnO_3$ system; $0.05 \leqslant x \leqslant 0.6$. The solid line denotes a true thermodynamic transition, the dashed line a change in the technical magnetic properties.

whereas the simple double exchange picture [yielding a fraction x of Mn^{4+} (saturation moment $3\mu_B$) and $1-x$ of Mn^{3+} (saturation moment $4\mu_B$)] would predict the *opposite* trend shown in the inset (as indeed would a rising fraction of lower oxidation state Mn ions). Such a result reflects the growing influence of competing interactions as x increases, resulting in a ground state which is not a uniform ferromagnet. Given the temperature of the lower boundary in Fig. 11, some comparisons with the canted state[38] in $PrAMnO_3$ (A=Ca, Sr, Ba,

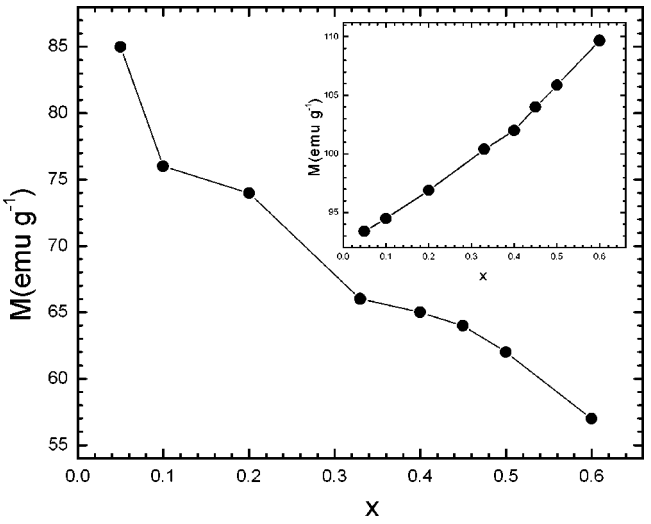

FIG. 11. The saturation moment M (in emu g^{-1}), estimated from magnetization curves taken at 4.2 K, plotted against the composition x. The inset shows the behavior predicted by the double-exchange model.

Na, K) occurring around 15% Mn^{4+} might be drawn. It should be emphasized, however, that there is no evidence that any such canting is coherent in the present system. Neutron scattering might provide further useful information in this regard, and could possibly resolve the origin of these competing interactions discussed in Sec. III B 1. The behavior shown in Fig. 11 nevertheless confirms that the conventional double-exchange picture alone cannot account comprehensively for the properties of this system, or indeed for the doped manganese perovskites in general, as first suggested by a detailed study[39] of their resistivities which, for the present system, are discussed below. Electronic phase separation into ferromagnetic and antiferromagnetic domains[2] could certainly account qualitatively for the magnetic properties discussed above. Difficulties arise, however, when discussing the transport behavior. Spontaneous electronic phase separation has been widely discussed in the context of a ferromagnetic, *metallic* state. Here the ferromagnetic state, by contrast, is insulating.

IV. TRANSPORT BEHAVIOR

The zero-field resistivity $\rho(T)$ of the three compositions investigated here show a semiconducting behavior—a monotonic increase in $\rho(T)$ with decreasing temperature—over the entire temperature range that can be accessed, $80 \leqslant T \leqslant 300$ K (with such a behavior precluding further measurements down to the liquid helium range). These data are quite similar to those reported[1] at lower x, and consequently are not reproduced here. These data have been fitted to forms consistent with the predictions for charge transport by small polaron hopping, viz.[40]

$$\rho(T) = \rho(0) T^n e^{E_a/k_B T}, \tag{7}$$

where the activation energy E_a is related to the polaron formation energy. With the exponent $n=1$, this equation represents such transport mediated not only in the adiabatic limit of such models—in contrast to the case with $n=3/2$ which corresponds to the nonadiabatic limit (both of which are discussed in more detail below)—but also the recent predictions for magnetic small polaron hopping specifically in a nonmetallic, phase separated picture.[3] The latter, however, involves electron transfer *between* magnetic polarons rather than the motion of polaronic entities themselves, as opposed to the percolation based approach of more widely accepted spontaneous phase separation models;[2] it has the advantage of providing an analytic form with which comparisons can be made, and applies to nonmetallic regimes, a dominant feature of the present system.

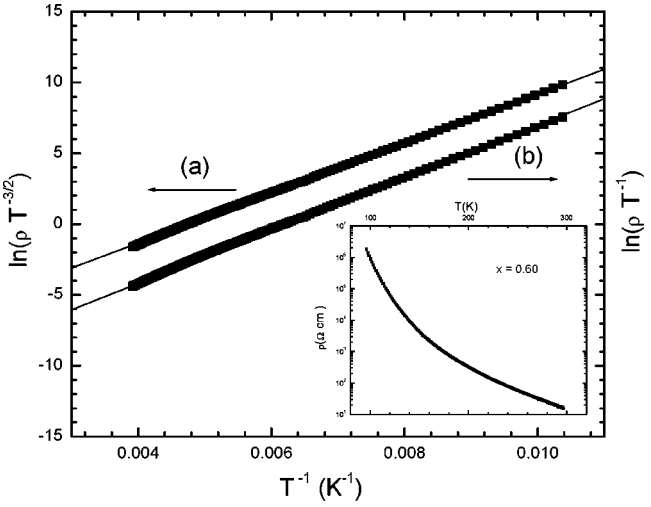

FIG. 12. A plot of the resistivity $\rho(T)$ (in Ω cm) against T^{-1} for the $x=0.6$ sample in a form consistent with Eq. (7) with (a) $n=1$ and (b) $n=3/2$. The inset shows ρ(T) plotted against temperature T (K) on a log-linear scale.

The high resistivity of these electron-doped samples below T_c precludes transport measurements there; fits only in the paramagnetic regime can thus be made. Indeed, experiments on these electron-doped specimens cover a larger temperature region of paramagnetism/magnetic disorder than those reported earlier.[1] Figure 12 reproduces representative fits for the $x=0.6$ sample, with the corresponding least-squares fitted parameters listed in Table II; either choice for n produces fits of comparable quality as judged by the associated standard errors. However, the appropriateness of either model can be appraised by a comparison of such fitted parameters with model assumptions or limits, specifically through $\rho(0)$ values. This prefactor $\rho(0)$ can be written as follows.[1]

(i) Adiabatic limit:

$$\rho(0) = \frac{k_B a}{g_d x(1-x) e^2 \Omega_0}. \tag{8}$$

Here a, the hopping distance, is generally identified with the (average) nearest neighbor Mn separation, while the numerical factor $g_d(\geqslant 1)$ reflects the topology of this hopping process (nearest neighbor, next neighbor, etc.). The factor $x(1-x)$ accounts for site occupation effects in the presence of strong on-site Coulomb repulsion.[41] The important parameter for comparative purposes is the attempt frequency Ω_0. In this adiabatic limit this is identified with a typical longitudi-

TABLE II. Parameters obtained from fits to the transport data above T_c.

x	Adiabatic/phase separation ($n=1$)			Nonadiabatic ($n=3/2$)		
	E_a (meV)	$\rho_0(\Omega$ cm)	Std Err	E_a (meV)	$\rho_0(\Omega$ cm)	Std Err
0.45	129	5.5×10^{-4}	0.11	139	2.2×10^{-5}	0.09
0.50	126	6.8×10^{-4}	0.17	132	3.1×10^{-5}	0.19
0.60	155	6.2×10^{-4}	0.14	162	9.1×10^{-6}	0.16

TABLE III. Model parameters $T > T_c$.

x	Adiabatic/phase separation		Nonadiabatic	
	Ω_0	l (Å)	Ω_0	$\lvert J\rvert$ (meV)
0.45	1.6×10^{11}	0.4	2.2×10^{11}	3
0.50	1.3×10^{11}	0.4	1.9×10^{11}	2.5
0.60	1.4×10^{11}	0.4	6.9×10^{11}	5

nal optical phonon frequency ω_0. Typically the latter assumes values of $\omega_0 = 10^{13} - 10^{14}$ Hz.[41,42]

(ii) Nonadiabatic limit:

$$\rho(0) = \frac{k_B a}{x(1-x)e^2\Omega_0}\frac{1}{T^{1/2}} = \frac{k_B a}{x(1-x)e^2}\frac{\hbar}{J^2}\left[\frac{4E_a k_B}{\pi}\right]^{1/2}. \tag{9}$$

Here two conditions need to be met for the applicability of this model/expression: (a) the electronic coupling/transfer matrix element $J \ll$ polaron formation energy (related, but not equal, to E_a), and (b)

$$\Omega_0 = \frac{J^2}{\hbar}\left[\frac{\pi}{4E_a k_B}\right]^{1/2} \ll \omega_0, \tag{10}$$

with ω_0 as above.

(iii) Phase-separation model:

$$\rho(0) = \frac{k_B}{128\pi v_0 (ce)^2 l^5}, \tag{11}$$

in which c represents the polaron density (identified with the carrier/hole density induced by doping), v_0 is a characteristic *magnon* frequency (rather than a phonon frequency), and l a tunnelling length.[3]

Table III summarizes estimates for Ω_0 and l found from these expressions for $\rho(0)$ and the corresponding fitted quantities (Table II). These Ω_0 estimates demonstrate conclusively that (i) the adiabatic limit is *not* appropriate in the paramagnetic phase of the electron-doped region of the present samples, and Ω_0 falls well below generally accepted values for ω_0 ($= 10^{13} - 10^{14}$ Hz); and (ii) the l values indicate that a phase-separation picture, within the specific formalism of Rakhmanov *et al.* for the *nonmetallic* regime, is also inconsistent with data on these systems. The listed estimates place $l < 1$ Å, not only substantially less than the Mn nearest neighbor separation (~ 3.9 Å) but also more than an order of magnitude smaller than model values ($l > 2a_0 \simeq 20$ Å, a_0 being the polaron radius[40,43]).

Having established the appropriateness of the nonadiabatic limit, Eq. (9) can be used to estimate $\lvert J\rvert$ from the fitted E_a and $\rho(0)$ values. These values for the electronic coupling parameter lie in the range 2.5–5 meV, consistent with the inequality $\lvert J\rvert \ll E_a$ on which Eq. (9) is based in these electron-doped samples, and comparable with estimates for this parameter found in the disordered phase of both hole-doped specimens[1] (2.5–16 meV) and $LaCrO_3$ (Refs. 1 and 41) ($\lvert J\rvert \simeq 8$ meV). The estimates are, however, almost an order of magnitude smaller than that found[1,41] from the high temperature phase of the undoped parent compound, $LaMnO_3$, $\lvert J\rvert \simeq 26$ meV. The high resistivity of these electron-doped manganites preclude transport measurements in the ordered phase, consequently the magnetoresistance could not be measured through T_c.

V. SUMMARY AND CONCLUSIONS

A summary of detailed measurements of both the linear and nonlinear magnetic response and the resistive behavior of electron-doped $La_{1-x}Mg_xMnO_3$ ($0.45 \leqslant x \leqslant 0.6$) is presented. The magnetic data clarify features of the phase diagram for this system proposed earlier, specifically that it displays a single conventional paramagnetic to ferromagnetic transition on cooling, with no subsequent reentrant transition to a spin-glass-like phase. Nevertheless, aspects of the magnetic behavior—both near T_c and at low temperature—exhibit features qualitatively consistent with electronic phase separation into ferromagnetic and antiferromagnetic domains, but not with a simple double exchange picture. In contrast with the majority of other systems, the ferromagnetic ground state remains insulating. Resistivity data (collected in the paramagnetic regime) are consistent with small polaron mediated charge transport, but are quantitatively inconsistent with the specific predictions for magnetic small polarons existing in a *nonmetallic* phase-separated environment.

ACKNOWLEDGMENTS

Support for this work from the Natural Sciences and Engineering Research Council (NSERC) of Canada and the University of Manitoba (J.H.Z.) is gratefully acknowledged.

[1] J. H. Zhao, H. H. Kunkel, X. Z. Zhou, and Gwyn Williams, J. Phys.: Condens. Matter **13**, 9349 (2001).

[2] A. Moreo, S. Yunoki, and E. Dagotto, Science **283**, 2034 (1999); A. Moreo, M. Mayr, A. Feiguin, S. Yunoki, and E. Dagotto, Phys. Rev. Lett. **84**, 5568 (2000); M. Mayr, A. Moreo, J. A. Verges, J. Arispe, A. Feiguin, and E. Dagotto, *ibid.* **86**, 135 (2001); E. Dagotto, T. Hotta, and A. Moreo, Phys. Rep. **344**, 1 (2001); J. Burgy, M. Mayr, V. Martin-Mayor, A. Moreo, and E. Dagotto, Phys. Rev. Lett. **87**, 277202 (2001).

[3] A. L. Rakhmanov, K. I. Kugel, Ya. M. Blanter, and M. Yu. Kagan, Phys. Rev. B **63**, 174424 (2001).

[4] L. C. LeGouillou and J. Zinn-Justin, Phys. Rev. B **21**, 3976 (1980).

[5] S. N. Kaul, J. Magn. Magn. Mater. **53**, 5 (1985); S. N. Kaul, A. Hofmann, and H. Kronmuller, J. Phys. F: Met **16**, 365 (1986); G. Williams, in *Magnetic Susceptibility of Superconductors and Other Spin Systems*, edited by R. A. Hein *et al.* (Plenum, New York, 1991), p. 475.

[6] I. Yeung, R. M. Roshko, and G. Williams, Phys. Rev. B **34**, 3456 (1986); R. M. Roshko and G. Williams, J. Appl. Phys. **55**, 1699 (1984); R. M. Roshko and G. Williams, J. Phys. F: Met **14**, 703 (1984).

[7] J. H. Zhao, T. Song, H. P. Kunkel, X. Z. Zhou, R. M. Roshko, and Gwyn Williams, J. Phys.: Condens. Matter **12**, 6903 (2000).

[8] J. H. Zhao, H. P. Kunkel, X. Z. Zhou, and Gwyn Williams, J. Phys.: Condens. Matter **13**, 5785 (2001).

[9] G. H. Rao, J. R. Sun, K. Barner, and N. Hamad, J. Phys.: Condens. Matter **11**, 1523 (1999).

[10] K. Dwight and N. Menyuk, Phys. Rev. **119**, 1470 (1960).

[11] S. de Brion, F. Ciorcas, G. Chouteau, P. Lejiay, P. Radaelli, and C. Chaillout, Phys. Rev. B **59**, 1304 (1999).

[12] I. S. Jacobs and J. S. Kouvel, Phys. Rev. **122**, 412 (1961).

[13] L. Q. Zheng and Q. F. Fang, J. Phys.: Condens. Matter **13**, 3411 (2001).

[14] T. R. N. Kutty and J. Philip, J. Phys.: Condens. Matter **12**, 7747 (2000).

[15] J. Fontcuberta, B. Martinez, A. Seffar, S. Pinol, J. L. Garcia-Munoz, and X. Obradors, Phys. Rev. Lett. **76**, 1122 (1996).

[16] J. Philip and T. N. R. Kutty, J. Phys.: Condens. Matter **11**, 8537 (1999).

[17] S. Chikazumi, *Physics of Ferromagnetism*, 2nd ed. (Clarendon, Oxford, 1997), p. 486.

[18] See, for example, B. R. Coles, B. V. B. Sarkissian, and R. H. Taylor, Philos. Mag. B **37**, 489 (1978); V. Cannella and J. A. Mydosh, Phys. Rev. B **6**, 4220 (1972); B. H. Verbeek, G. J. Nieuwenhuys, H. Stocher, and J. A. Mydosh, Phys. Rev. Lett. **40**, 586 (1978).

[19] H. E. Stanley, *Introduction to Phase Transitions and Critical Phenomena* (Clarendon, Oxford, 1971).

[20] H. P. Kunkel, R. M. Roshko, and G. Williams, Phys. Rev. B **37**, 5880 (1988).

[21] M. Compostrini, M. Hasenbusch, A. Pelissentto, P. Rossi, and E. Vicari, Phys. Rev. B **65**, 144520 (2002).

[22] J. H. Zhao, H. P. Kunkel, X. Z. Zhou, and Gwyn Williams, Phys. Rev. Lett. **83**, 219 (1999); A. Peles, H. P. Kunkel, X. Z. Zhou, and Gwyn Williams, J. Phys.: Condens. Matter **11**, 8111 (1999); P. A. Stampe and G. Williams, *ibid.* **10**, 8535 (1998); G. Williams, J. Alloys Compd. **326**, 36 (2001).

[23] A. B. Harris, J. Phys. C **7**, 1671 (1974).

[24] K. Binder and A. P. Young, Rev. Mod. Phys. **58**, 801 (1986); J. Hertz and K. A. Fischer, *Spin Glasses* (Cambridge University Press, New York, 1989).

[25] D. Sherrington and S. Kirkpatrick, Phys. Rev. Lett. **32**, 1792 (1975).

[26] X. L. Wang, J. Horvat, H. K. Liu, and S. X. Dou, J. Magn. Magn. Mater. **182**, L1 (1998); R. Mathieu, P. Nordblad, D. N. H. Nam, N. X. Phuc, and N. V. Khiem, Phys. Rev. B **63**, 174405 (2001), and references therein; J. Dho, W. S. Kim, and N. H. Hur, Phys. Rev. Lett. **89**, 027202 (2002).

[27] M. Gabay and G. Toulouse, Phys. Rev. Lett. **47**, 201 (1981).

[28] S. M. Dubiel, K. H. Fischer, Ch. Sauer, and W. Zinm, Phys. Rev. B **36**, 360 (1987).

[29] J. R. L. de Almeida and D. J. Thouless, J. Phys. A **11**, 983 (1978).

[30] R. N. Bhatt and A. P. Young, Phys. Rev. Lett. **54**, 924 (1985).

[31] T. Taniguchi, Y. Miyako, and J. L. Tholence, J. Phys. Soc. Jpn. **54**, 220 (1985); A. Tobo and A. Ito, *ibid.* **67**, 297 (1998).

[32] H. P. Kunkel and G. Williams, J. Phys. F: Met. Phys. **18**, 1271 (1988).

[33] A. G. Berndt *et al.*, Phys. Rev. B **52**, 10 160 (1995); J. Phys.: Condens. Matter **10**, 8535 (1998); H. P. Kunkel and G. Williams, J. Magn. Magn. Mater. **75**, 98 (1988); H. Ma *et al.*, J. Phys.: Condens. Matter **3**, 5563 (1991).

[34] K. Kornik, R. M. Roshko, and G. Williams, J. Magn. Magn. Mater. **81**, 323 (1989).

[35] A. Maignan, C. Martin, G. Van Tendeloo, M. Hervieu, and B. Raveau, Phys. Rev. B **60**, 15 214 (1999). While the average A site radius $\langle r_A \rangle = 0.105$ nm ($x = 0.5$) is smaller here than in the study by Maignan *et al.*, it is relevant to point out that a complete suppression of the metal-insulator transition in the present system is in agreement with the global stability index model of G. H. Rao, K. Barner, and I. D. Brown, J. Phys.: Condens. Matter **10**, L757 (1998) for which I. D. Brown (private communication) calculated the corresponding index $R1 = 0.519$ at $x = 0.33$, placing that sample in the crossover TMI region between FMM and FMI ground states.

[36] T. Song, R. M. Roshko, and E. D. Dahlberg, J. Phys.: Condens. Matter **13**, 3443 (2001); J. H. Zhao, T. Song, H. P. Kunkel, X. Z. Zhou, G. Williams, and R. R. Roshko, J. Appl. Phys. **89**, 7248 (2001).

[37] P. Schiffer, A. P. Ramirez, W. Bao, and S. W. Cheong, Phys. Rev. Lett. **75**, 3336 (1995); Y. Tomioka, A. Asamitsu, H. Kuwahara, and Y. Moritomo, Phys. Rev. B **53**, R1689 (1996).

[38] Z. Jirak, J. Hejtmanek, E. Pollert, M. Marysko, M. Dlouha, and S. Vratislav, J. Appl. Phys. **81**, 5790 (1997).

[39] A. J. Millis, P. B. Littlewood, and B. T. Shraiman, Phys. Rev. Lett. **74**, 5144 (1995); A. J. Millis, B. I. Shraiman, and R. Mueller, *ibid.* **77**, 175 (1996); Q. Li, J. Zang, A. R. Bishop, and C. M. Soukoulis, Phys. Rev. B **56**, 4541 (1997).

[40] D. Emin and T. Holstein, Ann. Phys. (N.Y.) **53**, 439 (1969); D. Emin and N. L. H. Liu, Phys. Rev. B **27**, 4788 (1983); M. Jaime, H. T. Hardner, M. B. Salamon, M. Rubinstein, P. Dorsey, and D. Emin, Phys. Rev. Lett. **78**, 951 (1997); M. Jaime and M. B. Salamon, in *Physics of Manganites*, edited by T. A. Kaplan and S. D. Mahanti (Plenum, New York, 1999); J. P. Franck, I. Issac, Weimim Chen, J. Chrzanowski, and J. C. Irwin, Phys. Rev. B **58**, 5189 (1998); D. C. Worledge, L. Mieville, and T. H. Geballe, *ibid.* **57**, 15 267 (1998).

[41] R. Raffaelle, H. U. Anderson, D. M. Sparlin, and P. E. Parris, Phys. Rev. B **43**, 7991 (1991); M. Jaime, M. B. Salamon, M. Rubinstein, R. E. Treese, J. S. Horwitz, and D. B. Chrisey, *ibid.* **54**, 11 914 (1996).

[42] J. C. Philips, in *Physics of High-T_c Superconductors* (Academic Press, San Diego, 1989).

[43] M. Yu Kagan, D. I. Khomshii, and M. V. Mostovoy, Eur. Phys. J. B **12**, 217 (1999).